Mechanical Systems and Signal Processing 109 (2018) 134–149

Contents lists available at ScienceDirect

Mechanical Systems and Signal Processing

journal homepage: www.elsevier.com/locate/ymssp

Multi-dimensional signal processing and mode tracking approach for guided wave based damage localization in X-COR sandwich composite

Guoyi Li [a], Aditi Chattopadhyay [b,*]

[a] School for Engineering of Matter, Transport and Energy, Arizona State University, Tempe, AZ, USA
[b] Mechanical and Aerospace Engineering, School for Engineering of Matter, Transport and Energy, Arizona State University, Tempe, AZ, USA

ARTICLE INFO

Article history:
Received 29 August 2017
Received in revised form 15 January 2018
Accepted 25 February 2018

Keywords:
Ultrasonic guided waves
X-COR sandwich composites
Structural health monitoring
Signal processing
Wave mode tracking
Damage localization

ABSTRACT

This paper presents a real-time signal processing and damage localization framework for ultrasonic guided wave based structural health monitoring of X-COR sandwich composites with a reference-free perspective. The high attenuation nature of X-COR composite significantly limits the ability to detect damage-induced reflected waveforms. Therefore, a novel multi-dimensional signal processing technique, coupled with a mode tracking approach for identifying trajectories and locating wave sources of all wave modes, including damage-induced converted modes, is proposed. The developed framework is experimentally validated using two internal damage scenarios: facesheet delamination and foam core separation. Results indicate that the framework offers not only high accuracy for locating internal damage positions, but also insights into guided wave propagation behaviors in highly complex composites such as the X-COR sandwich composite.

1. Introduction

Advanced light-weight composite structures, such as the X-COR sandwich composite, possess excellent durability, specific strength and stiffness, damping and impact properties that are all advantageous for mechanical and aerospace applications [1,2]. Specifically, the Z-pin of X-COR sandwich composite, which penetrates both the foam core and facesheets, improves the through-thickness compression strength of the structure [3]. However, the architectural complexities associated with pin-penetrated foam core and difficult-to-detect damage scenarios, such as facesheet delamination and foam core separation, can compromise the safety and reliability of X-COR composites. Real-time inspection and monitoring of the operational health of X-COR sandwich composites has received little attention to date. A robust structural health monitoring (SHM) methodology, therefore, is needed to effectively identify and localize the damage states in these advance composites, and to provide meaningful information for estimating their residual life.

Thus far, among SHM technologies, ultrasonic guided wave (UGW) based techniques have proven to be very effective, primarily due to their ability to propagate long distances with minimum energy loss, resulting in a large inspection area [4,5], and capability of interrogating structures in the through-thickness direction. As such, UGW based damage detection and localization techniques are widely used to inspect the structural health of materials including carbon fiber reinforced composites [6]. The guided wave based detection and localization algorithms can be generally classified into two classes: forward

* Corresponding author at: Arizona State University, Tempe, AZ 85287-6106, USA.
E-mail address: aditi@asu.edu (A. Chattopadhyay).

https://doi.org/10.1016/j.ymssp.2018.02.039
0888-3270/

algorithm and inverse algorithm. The ellipse based method, which is the most widely used algorithm [7–10], is a forward algorithm, which utilizes the time of flight (ToF) information of UGW. ToF is defined as the time lag between the excitation wave mode and the damage-induced reflected wave mode so that a damage ellipse, which contains all possible damage locations, can be further constructed. Diaz Valdes and Soutis (2002) [11], for example, used a pulse-echo method for localizing the delamination in a carbon fiber composite panel. Their results showed that the reflected wave from the delaminated region could be detected, and delamination was successfully localized. In order to explicitly consider the effects of temperature on the accuracy of damage localization, Neerukatti et al. (2015) [12] developed a fully probabilistic methodology based on a temperature compensation algorithm. This method was experimentally validated and showed marked improvements over the traditional ellipse based method. Another ellipse based method, phased array technique, was implemented by Giurgiutu (2006) [13] to develop an embedded ultrasonic structural radar (EUSR) algorithm, and this method showed high accuracy in predicting crack and corrosion in metallic materials. In addition, Kessler et al. (2002) [14] showed that a frequency response method is also an effective tool for damage detection in composite materials. Zak et al. [15] demonstrated a vibration method that detects closing delamination by analyzing the vibration modes and investigating the effects of delamination on the response frequencies. Similarly, Kim et al. [16] developed a modal-strain-based damage detection method for laminated composite structures based on smooth transition of displacements. Contrary to time or frequency domain analysis, high dimensional methods, which investigates guided wave signals in multiple representative domains simultaneously, have shown success in detecting delamination in composite materials; these high dimensional methods typically involve high dimensional signal processing techniques such as time-frequency analysis, frequency-wavenumber analysis and time-space analysis. Liu et al. (2012) [17] implemented time-frequency analysis to identify and localize the damage in a stiffened composite panel. Moreover, a scattering based wave packet tracing method to quantify the group and phase velocities in the time-space domain was developed by Kim and Chattopadhyay [18]. This method was incorporated into the ToF based localization algorithm and showed high accuracy in localizing and quantifying damage in aluminum plates. Using scanning laser Doppler measurements, Michaels et al. (2011) [19] developed a frequency-wavenumber domain analysis, wherein the time-space domain was transformed through a two dimensional Fourier transform in order to detect delamination in composites. Yu and Tian (2013) [20] used space-frequency-wavenumber domain analysis to study how the frequency-wavenumber relation varies in the spatial domain.

The inverse method, which is another class of damage detection algorithm, quantifies the damage in the composite. Yam et al. (2003) [21] developed a vibration based method using an artificial neural network to map the relationship between output signals and damage size or location. Image processing based techniques [22] are also available for nondestructive evaluation (NDE) purposes. For X-COR sandwich composites, as presented in this study, Neerukatti et al. (2016) [23] developed a hybrid NDE/SHM method for damage detection. Their results indicated that ultrasonic C-scan and flash thermography can successfully detect, localize, and quantify internal damage, and that the presence of damage can lead to mode conversion when using UGW based SHM technique.

In spite of the aforementioned advances, UGW based damage localization methods continue to experience many challenges. As suggested by Diamanti et al. (2004) [24], UGWs have greater attenuation due to the presence of a low-stiffness core than those propagating in traditional metallic and composite materials, challenging the detection of damage-induced reflected waves. Li et al. (2017) [25] showed that the presence of Z-pins in X-COR sandwich composites made the signals received by the sensors more complex, i.e., inducing nonlinearity and larger attenuation. In addition, Neerukatti et al. (2016) [23] claimed that the sensor placement was a critical issue for damage detection in X-COR sandwich composites. Similarly, as will be discussed in Section 2.1 of this paper, it is difficult to detect the reflected wave that is induced by delamination in X-COR sandwich composites due to the highly attenuation fact of host structure. This, in turn, restricts the utility of many traditional ellipse based methods. On the other hand, the size of the transducers attached on the structures used for real-time SHM presents significant challenges for both the spatial sampling rate of Fourier transform for wavenumber-frequency analysis and the image resolution of image processing based algorithms. Moreover, a reference-free localization algorithm is highly desirable because it eliminates the need for a 'healthy' baseline, thereby reducing the fabrication cost associated with advanced composite structures such as X-COR sandwich composites. Finally, it is important to note that the concept of a 'healthy' baseline is often misleading due to the presence of manufacturing induced flaws.

In this paper, a novel multi-dimensional signal processing and mode tracking approach with a reference-free perspective is developed for the damage identification and localization in the media with large attenuation fact. In current experimental methodology, the reflected wave cannot be easily detected due to the issues of X-COR sandwich composite mentioned above. In this work, an alternative approach is proposed, where, instead of detecting reflected waves, the damage-induced converted wave modes are used as indicators of internal damages [17]. An advanced signal processing technique called matching pursuit decomposition (MPD) [26] is used to effectively de-noise the signals in the time-frequency domain. The de-noised signals are then processed using a Hilbert transform based envelope detection technique [27] to isolate wave modes from each other in the time domain and to construct the time-space representation (TSR) using the spatial information of the sensors. An iterative mode tracking algorithm is then developed to track all the wave mode trajectories in the time-space domain, localizing the wave sources while providing a fundamental understanding of the mode conversion mechanism involved in the UGW based SHM framework. Then, X-COR sandwich panels with two artificially seeded damage scenarios, i.e., facesheet delamination and foam core separation, are used to validate the developed framework.

The remainder of this paper is organized as follows. Section 2 introduces the mathematical formulations of multi-dimensional signal processing and the mode tracking approach for damage localization. Section 3 describes the experimental

details, including specimen and sensor specifications, sensor deployment, and data acquisition. The results associated with relevant discussions are shown in Section 4 and concluding remarks of the current research work are summarized in Section 5.

2. Multi-dimensional signal processing and mode tracking approach

A demonstrative experiment that shows the challenges of detecting reflected waves induced by top facesheet delamination in an X-COR sandwich panel is presented in Section 2.1. A multi-dimensional signal processing technique for constructing an effective TSR that shows the relationship between ToF, amplitudes, and spatial information of wave modes contained in sensing signals is introduced in Section 2.2. The mathematical formulation of the mode tracking algorithm that interprets signal features and locates damage positions are shown in Section 2.3. A schematic of the computational framework is shown in the Fig. 1.

2.1. Challenges in detecting reflected waves

A demonstrative experiment that shows the challenges of detecting reflected waves induced by top facesheet delamination in an X-COR sandwich panel and the subsequent problems of using the traditional ellipse based damage localization

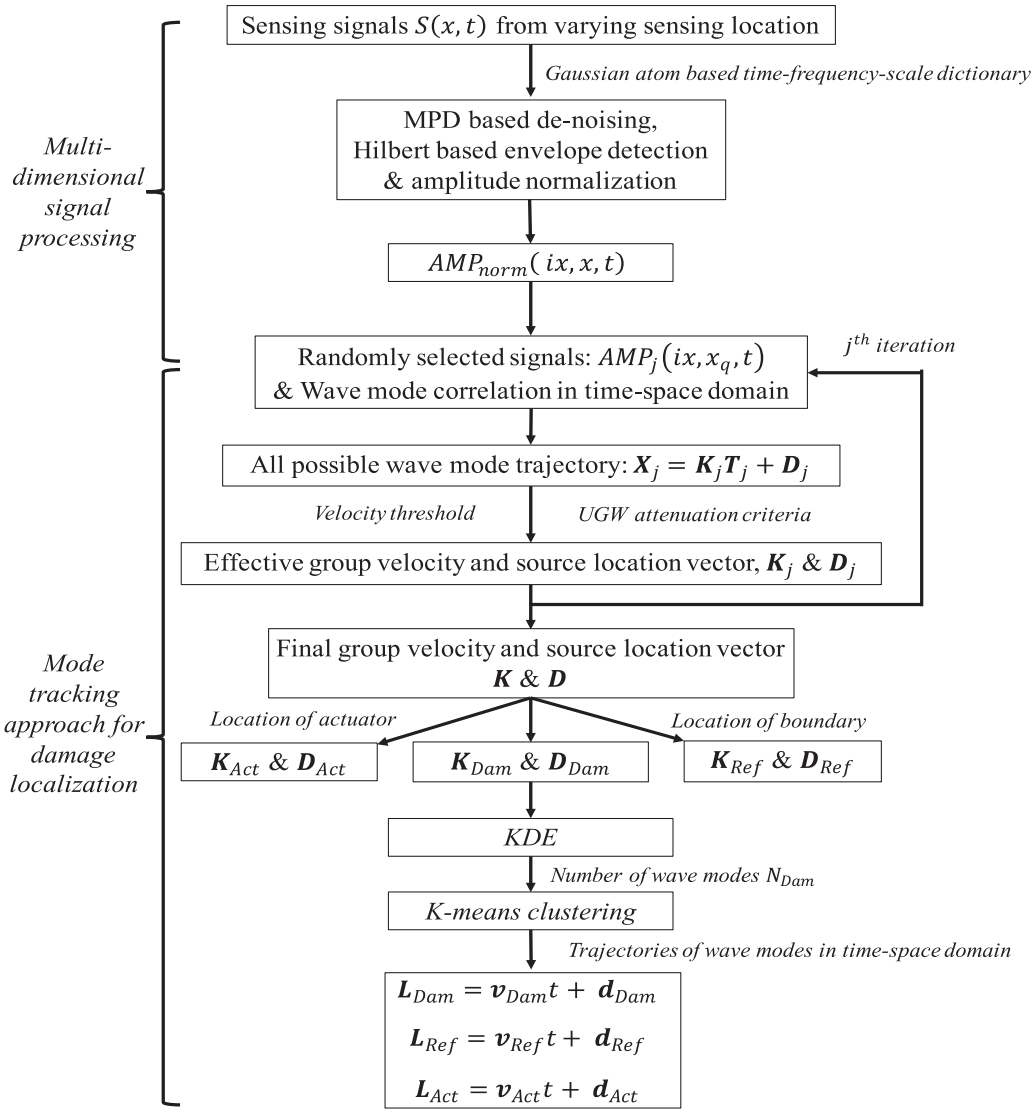

Fig. 1. Computational schematic of multi-dimensional signal processing and mode tracking approach for damage localization.

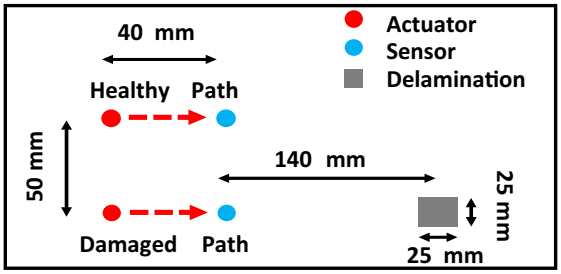

Fig. 2. Experimental schematic for demonstrating difficulty in detecting damage-induced reflected wave.

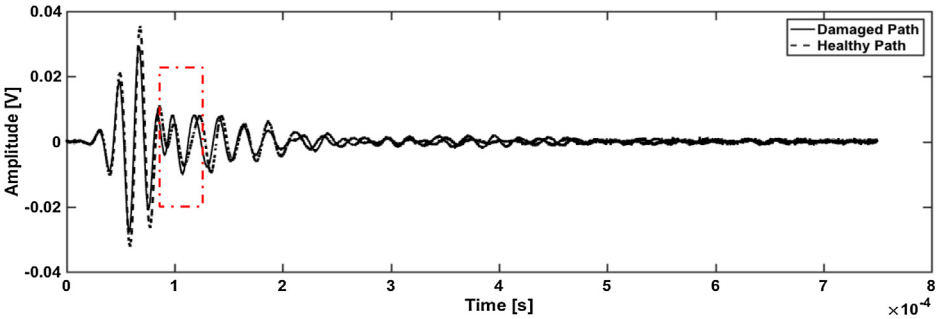

Fig. 3. Signal comparison between healthy path (dash line) and damaged path (solid line); red square shows where the reflected wave should appear. (For interpretation of the references to colour in this figure legend, the reader is referred to the web version of this article.)

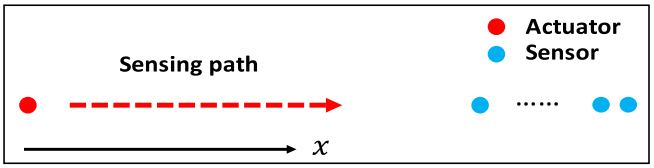

Fig. 4. Demonstration of the architecture of a single sensing path.

methods is presented. As shown in Fig. 2, four macro-fiber composite (MFC) transducers were attached to the surface of a X-COR sandwich panel; two MFCs were used as actuators (in red) and the other two MFCs were used as sensors (in blue), forming two sensing paths: a healthy path (with no damage) and a damaged path. A plastic Teflon sheet was seeded at the mid-layer of the facesheet in the damaged path, mimicking the presence of facesheet delamination. A five-cycle cosine tone burst under excitation frequencies of 10–110 kHz was applied in order to capture the damage-induced reflected wave. In this set up, while the reflected wave could not be detected under the aforementioned range of excitation frequencies, for demonstrative purposes, we were able to instead compare the signals received from the healthy path and the damaged path under a 50 kHz excitation frequency. As shown in Fig. 3, there was no significant difference observed between the signals received by the healthy path (dash line) and damaged path (solid line), indicating that no additional wave modes were found in the signal received by the sensor in the damaged path. Based on experiments [32], the group velocity of first wave mode was 4083 m/s, which would be the group velocity of the first reflected wave received by the sensor if it was detectible, and its location in time domain is marked by the red dash-line box in Fig. 3. This experiment thus confirmed that it is necessary to develop a damage detection and localization framework that does not fully rely on the damage-induced reflected wave.

2.2. Multi-dimensional signal processing

In order to accurately and efficiently localize the internal damage while providing mechanistic insights into UGW and damage interactions, a sensor array was used for tracking the trajectories of wave modes in each sensing path. The sensing architecture is demonstrated in Fig. 4, where each sensing path comprised an actuator and multiple evenly spaced sensors; signals were recorded by each sensor simultaneously. A time-frequency based MPD algorithm that extracts the harmonic wave mode was then applied to de-noise the sensing signal.

The signal received by the sensor is defined as $S(x,t)$, where x is the location of the sensor in the sensing path, as shown in Fig. 4, and t is the time. Signal $S(x,t)$ is decomposed by a linear combination of scale-time-frequency atoms, and the de-noised signal, $S_{de-noised}(x,t)$, is then expressed as

$$S_{de-noised}(x,t) = \sum_{k=0}^{M-1} \alpha_k(x) g_k(x,t) + r_M(x,t) \tag{1}$$

and

$$r_M(x,t) = S(x,t) - \sum_{k=0}^{M-1} \alpha_k(x) g_k(x,t) \tag{2}$$

where $(M-1)$ is the number of iterations, $\alpha_k(x)$ is the coefficient of scale (also known as coefficient of expansion), $g_k(x,t)$ is the basis function selected from the atom dictionary $\mathbb{D}$, and $r_M(x,t)$ represents the residual signal after $(M-1)^{th}$ MPD iterations. In order to decompose the signal effectively while maintaining its computational efficiency, an advanced Gaussian atom [28] dictionary is designed and expressed as

$$\mathbb{D} = \left(\frac{8 s_l}{\pi}\right)^{1/4} e^{-s_l (t-\tau_n)^2} \cos(2\pi \upsilon_m) \tag{3}$$

where s_l $(l = 1, \ldots, l_{max})$, τ_n $(n = 1, \ldots, n_{max})$ and υ_m $(m = 1, \ldots, m_{max})$ are the scale shift, time shift, and frequency shift, respectively, that define the matching pursuit region. The basis function in each iteration is the atom that has the maximum correlation with the signal $S_{de-noised}(x,t)$, and can be expressed as

$$(g_k(x,t)) = \underset{g_k(t,s_l,\tau_n,\upsilon_m)\in\mathbb{D}}{\operatorname{argmax}} \left| \int_{-\infty}^{\infty} r_M(x,t) g_k(t,s_l,\tau_n,\upsilon_m) dt \right| \tag{4}$$

and the expansion coefficient is

$$\alpha_k(x) = \int_{-\infty}^{\infty} r_M(x,t) g_k(x,t) dt \tag{5}$$

Through the MPD methodology, the harmonic waveforms wherein sensing signals can be efficiently extracted, while the noise being filtered because of less correlation with the atoms in the designed dictionary. A Hilbert based envelope detection algorithm is then applied to isolate wave modes. This algorithm improves the efficiency of the damage localization [29] in the time-space domain that will be discussed in Section 2.3. The envelope of wave mode can be found by the absolute value of the analytical signal, $S_{Analytical}(x,t)$, whose real part is defined as the original de-noised signal; the imaginary part is the Hilbert transform of the de-noised signal. The analytical signal can be written as follows

$$S_{Analytical}(x,t) = S_{de-noised}(x,t) + i\mathcal{H}(S_{de-noised})(x,t) \tag{6}$$

where $\mathcal{H}(\cdot)$ is the Hilbert transform that can be explicitly expressed as

$$\mathcal{H}(S_{de-noised})(x,t) = -\frac{1}{\pi} \lim_{\varepsilon \to 0} \int_{\varepsilon}^{\infty} \frac{S_{Analytical}(x,t+\tau) - S_{Analytical}(x,t-\tau)}{\tau} d\tau \tag{7}$$

The mode envelope, $ENV(x,t)$, can be expressed as

$$ENV(x,t) = |S_{Analytical}(x,t)| = \sqrt[2]{S^2_{de-noised}(x,t) + \mathcal{H}^2(S_{de-noised}(x,t))} \tag{8}$$

which represents the signals constructed in the time space domain by the envelope, thus preserving not only the amplitude information of all the modes present in the signals, but also the spatial relationship of sensors. The vector of local maxima, referred as the peak of wave mode, is defined as $AMP(ix,x,t)$, where $ix = 1, 2, \ldots, i$ indicates the i^{th} peak in the sensing signal at location x. This can be found through the first and second derivatives of the envelope vector $ENV(x,t)$. In order to identify the direction of each mode, the amplitudes of wave modes that obtained from sensors at different sensing locations need to be compared. Therefore, the amplitude vector $AMP(ix,x,t)$ is normalized by the largest amplitude in the entire time-space domain (i.e., the maximum value of three dimensional $AMP(ix,x,t)$) and is expressed as follows.

$$AMP_{norm}(ix,x,t) = \frac{AMP(ix,x,t)}{AMP_{max}} \tag{9}$$

2.3. Mode tracking approach for damage localization

The UGW modes of each sensor are isolated in the time-space domain and represented by $AMP_{norm}(ix,x,t)$ using Eq. (9). The next step was to interpret the relationship between the wave modes from the sensors at different sensing locations. For this purpose, a novel mode tracking approach that correlates the peak of wave modes in time-space domain was developed. The following hypotheses were proposed for all the wave modes: (1) The derivative of trajectory in time-space domain is

defined as the wave mode velocity, i.e., group velocity; (2) The intersection of wave mode trajectory with the spatial direction at time zero in time-space domain indicates the source location of the wave mode; (3) The wave exhibits attenuation behavior, i.e., amplitudes continuously decrease with respect to propagation distance; (4) Ultrasonic feature, wherein group velocities are faster than the speed of sound in the air (>343 m/s) is maintained; (5) The converted modes maintain the characteristics of a guided wave (e.g., constant velocity) and can be recorded using surface bonded piezoelectric sensors.

In order to address the uncertainties introduced by various sources such as sensors, data acquisition process and feature extraction algorithm, an iterative computational scheme was also implemented. Three sensing locations were selected at each iteration so that the trajectories of wave modes from the three selected sensors were identified by mode peak correlation. In the j^{th} iteration, three sensors were randomly picked from the amplitude array $AMP_{norm}(ix, x, t)$. The selected amplitude vector from sensor at location x_1, x_2 and x_3 of j^{th} iteration is expressed as $AMP_j(ix, x_q, t)$, where $q = 1, 2, 3$. The intersection vector, $d_j^*(u, v)$, defined as the intersection of wave mode trajectory with the spatial direction at time zero in time-space domain indicating the wave source location, and the corresponding slope vector, i.e., the group velocity vector, defined as $k_j^*(u, v)$, can be expressed using linear combination of wave modes, associated with sensors at location x_1 and x_2, as follows.

$$d_j^*(u, v) = \frac{x_2 t_{1v} - x_1 t_{2u}}{t_{2v} - t_{1u}} \tag{10}$$

and

$$k_j^*(u, v) = \frac{x_2 - x_1}{t_{2v} - t_{1u}} \tag{11}$$

where t_{1u} and t_{2v} are the ToF of u^{th} peak of the first sensor, x_1, and the ToF of v^{th} peak of the second sensor, x_2, respectively. By utilizing $k_j^*(u, v)$ and $d_j^*(u, v)$, the time-domain interaction at sensor location x_3, $Int_j^*(u, v)$, can be found as

$$Int_j^*(u, v) = \frac{x_3 - d_j^*(u, v)}{k_j^*(u, v)} \tag{12}$$

The peak at x_3 that corresponding to the trajectory found through peaks at x_1, t_{1u} and x_2, t_{2v} is defined as $AMP_j(ix_3, x_3, t_w)$ and the location can be found by

$$(x_3, t_w) = \underset{|Int_j^*(u,v) - t_w| < t_{\min}}{\operatorname{argmin}} |Int_j^*(u, v) - t_w| \tag{13}$$

where t_w is the time of the location of peak containing in signals from the third sensor, which has the minimum distance to the time-space relation established by the sensor at location x_1 and x_2, and threshold t_{min} is defined based on the fourth hypothesis. Then, a linear regression model is defined as

$$\boldsymbol{X}_j = \boldsymbol{K}_j \boldsymbol{T}_j + \boldsymbol{D}_j \tag{14}$$

when satisfying

$$\frac{AMP_j(i3, x_3, t_w) - AMP_j(i2, x_2, t_v)}{AMP_j(i2, x_3, t_w) - AMP_j(i1, x_1, t_u)} > 0 \tag{15}$$

where $\boldsymbol{X}_j = [x_1\ x_2\ x_3]^T$, $\boldsymbol{T}_j = [t_u\ t_v\ t_w]^T$, $\boldsymbol{K}_j$ and $\boldsymbol{D}_j$ are the wave mode location vector, wave mode ToF vector, group velocity vector, and source location vector at j^{th} iteration, respectively. The criteria in Eq. (15) is defined based on the third hypothesis that improves computational efficiency and accuracy. The vectors $\boldsymbol{K}_j$ and $\boldsymbol{D}_j$ are found through

$$(\boldsymbol{K}_j, \boldsymbol{D}_j) = \operatorname{argmin}(\boldsymbol{X}_j - (\boldsymbol{K}_j \boldsymbol{T}_j + \boldsymbol{D}_j))^2 \tag{16}$$

and they are further used to construct the final group velocity and source location vector, $\boldsymbol{K}$ and $\boldsymbol{D}$, which can be expressed as

$$\boldsymbol{K} = [\boldsymbol{K}_1, \boldsymbol{K}_2, \boldsymbol{K}_3, \ldots \boldsymbol{K}_J] = [k_1 \quad k_2 \quad k_3 \quad \ldots \quad k_T] \tag{17}$$

and

$$\boldsymbol{D} = [\boldsymbol{D}_1, \boldsymbol{D}_2, \boldsymbol{D}_3, \ldots \boldsymbol{D}_J] = [d_1 \quad d_2 \quad d_3 \quad \ldots \quad d_T] \tag{18}$$

where J is the number of iterations, and T is the total number of wave modes in the velocity and source location final vector.

A physics-based clustering method is applied to classify the locations in the source location vector $\boldsymbol{D}$ based on the known locations of actuators and boundaries. The clustering method is briefly described next. If the element d is located in the actuating region,

$$\boldsymbol{D}_{Act} = [d_1 \quad d_2 \quad d_3 \quad \ldots \quad d_a] \tag{19}$$

the corresponding group velocity vector can be expressed as

$$\boldsymbol{K}_{Act} = [k_1 \quad k_2 \quad k_3 \quad \ldots \quad k_a] \tag{20}$$

If the element d is located at or outside the panel boundaries, the corresponding wave modes are identified as boundary reflected waves,

$$\boldsymbol{D}_{Ref} = [d_1 \quad d_2 \quad d_3 \quad \dots \quad d_r] \tag{21}$$

so that the group velocity vector is

$$\boldsymbol{K}_{Ref} = [k_1 \quad k_2 \quad k_3 \quad \dots \quad k_r] \tag{22}$$

If the element d is located neither at actuating region nor outside the panel boundaries, it will be regarded as the location of damage,

$$\boldsymbol{D}_{Dam} = [d_1 \quad d_2 \quad d_3 \quad \dots \quad d_q] \tag{23}$$

and the corresponding group velocity vector can be expressed as

$$\boldsymbol{K}_{Dam} = [k_1 \quad k_2 \quad k_3 \quad \dots \quad k_q] \tag{24}$$

where a, r and d are number of velocities or source location values from actuating region, reflecting region and damaged region, respectively, which satisfies the relation $a + r + q = T$.

For the purpose of locating internal damage while achieving an understanding of UGW behavior, all the wave modes that are present in each velocity vector are investigated individually. Therefore, these modes are clustered based on the dispersion nature of UGW, namely, different wave modes possess different group velocities. Because each iteration processes data with different sensor combinations, the mode velocities in each iteration will not be the same due to experimental uncertainties. Furthermore, the number of modes in group velocity vectors $\boldsymbol{K}_{Act}$, $\boldsymbol{K}_{ref}$ and $\boldsymbol{K}_{Dam}$ are still unknown, which complicates the clustering process. Therefore, prior to clustering, the number of modes present in each vector is identified through the number of peaks present in the velocity distribution function, which is then regarded as the number of clusters in the clustering step. A K-means clustering is then applied to identify the source location of each mode.

As an example, an algorithm of group velocity clustering for $\boldsymbol{K}_{Dam}$ is presented; the algorithms for $\boldsymbol{K}_{Act}$ and $\boldsymbol{K}_{ref}$ are identical. A kernel density estimator (KDE) [30], $f_k(v)$, is assigned to estimate the probability density function (PDF) of $\boldsymbol{K}_{Dam}$. Because the KDE is a non-parametric density estimator, the number of wave modes is no longer a required known parameter. $f_k(v)$ is expressed as

$$f_k(v) = \frac{1}{qh}\sum_{i=1}^{r} F_K\left(\frac{v - v_i}{h}\right) \tag{25}$$

where q is the number of velocity values contained in $\boldsymbol{K}_{Dam}$, v is the variable representing wave velocity, and $F_K(\cdot)$ is the kernel function. In this study, the normal kernel function is chosen because of its accuracy and computational efficiency. The number of peaks in the distribution, N_{Dam}, which represents the number of presented wave modes, is found using the following derivative formula:

$$\frac{\partial f_k(v)}{\partial v} = 0 \tag{26}$$

when

$$\frac{\partial^2 f_k(v)}{\partial^2 v} < 0 \tag{27}$$

Thus, the velocity of each mode present in sensing signal can be found by applying K-means clustering [31] as follow, while defining the velocity vector as $\boldsymbol{v}_{Dam}$.

$$(\boldsymbol{c}^R, \boldsymbol{v}_{Dam}) = \operatorname{argmin} \frac{1}{r}\sum_{i=1}^{q} ||v_i - \boldsymbol{v}_{\boldsymbol{c}^i}||^2 \tag{28}$$

where $\boldsymbol{c}^R$ is index of cluster $(1, 2, \dots, N_{Dam})$ of that v_i is currently assigned, and $\boldsymbol{v}_{\boldsymbol{c}^i}$ is the cluster centroid of cluster to which example v_i has been assigned. The source location corresponding to each cluster is defined by the mean value of source locations in $\boldsymbol{D}_{Dam}$, whose velocities belong to this cluster. The vector $\boldsymbol{d}_{Dam}$ is defined as the final source location for the scanning region. Thus, the trajectories of all the damage-induced modes can be expressed in the time-space domain through the equation below.

$$\boldsymbol{L}_{Dam} = \boldsymbol{v}_{Dam} t + \boldsymbol{d}_{Dam} \tag{29}$$

where t and $\boldsymbol{L}_{Dam}$ are the time and corresponding space location of wave modes, respectively. Similarly, the trajectories of all the boundary reflected wave modes and actuated wave modes can be found and expressed as

$$\boldsymbol{L}_{Ref} = \boldsymbol{v}_{Ref} t + \boldsymbol{d}_{Ref} \tag{30}$$

and

$$\boldsymbol{L}_{Act} = \boldsymbol{v}_{Act} t + \boldsymbol{d}_{Act} \tag{31}$$

where $\boldsymbol{v}_{Ref}$, $\boldsymbol{v}_{Act}$, $\boldsymbol{d}_{Ref}$, $\boldsymbol{d}_{Act}$, $\boldsymbol{L}_{Ref}$ and $\boldsymbol{L}_{Act}$ are velocity vector of reflected wave mode, velocity vector of actuated wave mode, source location vector of reflected wave mode, source location vector of actuated wave mode, space location of reflected wave modes, and space location of actuated wave modes, respectively. In addition, the error for each mode is defined as

$$Err = \left| \frac{d_{predicted} - d_{Actual}}{d_{Actual}} \right| \times 100\% \tag{32}$$

where $d_{predicted}$ and d_{Actual} are the predicted and actual locations of damage, actuators and boundary.

3. Experimental setup

The X-COR sandwich panels were manufactured at Boeing facility in Mesa, Arizona, U.S. The dimensions of the panels were 450 mm × 450 mm × 13 mm. The panels were constructed using quasi-isotropic carbon fiber composite facesheets (top and bottom), and internal X-CORs containing polyurethane foam and evenly distributed carbon pins with an inclining angle of 20° that penetrated both the top and bottom facesheets. Two damage scenarios, facesheet delamination and foam core separation, were considered for validating the developed framework. The sizes of delamination were defined based on the critical defect sizes in composite structures [11]. Therefore, additional 19.05 mm × 19.05 mm folded Teflon layers were inserted between the second and third layers of the four-layer top facesheet to provide an air gap that could simulate the interply of delaminations. The pins in this region were trimmed to ensure that there was no adhesion. Folded Teflon layers of the same sizes, using the same insertion technique, were placed between the top facesheet and X-COR, thus representing the foam core separation damage scenario.

The locations of damage were predefined and validated using NDE techniques, including flash thermography and C-scan, as presented in our previous work [23]. The NI PXI 14-bit 100 MS/s arbitrary wave generator (AWG) and 12-bit 60 MS/s

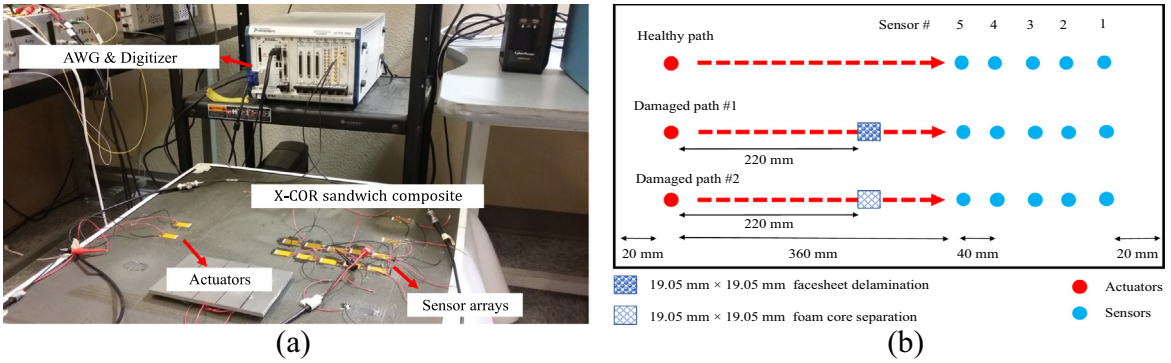

Fig. 5. Illustration of (a) experimental setup and (b) schematic of test plate.

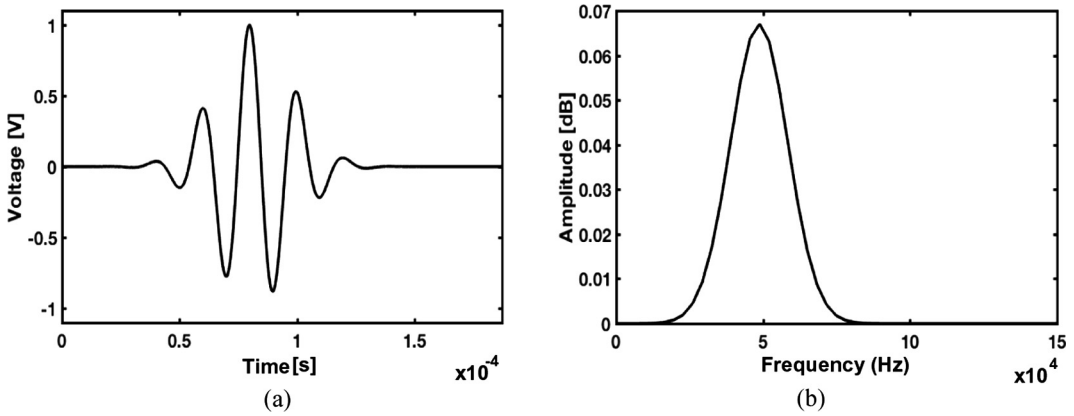

Fig. 6. Illustration of excitation signal waveform with its frequency spectrum under a 50 kHz excitation frequency.

digitizer, shown in Fig. 5(a), were used to generate the 5-cycle cosine tone burst excitation signal and to collect signals from each sensor with a 20 MHz sampling frequency. The waveform and corresponding frequency spectrum under a 50 kHz excitation frequency are shown in Fig. 6. MFCs from Smart Material Corp., type M 2814 P2, were used as sensors and actuators. The MFC arrays were bonded on the top surface using super glue from StewMac Inc.; each array comprised an actuator and five equally spaced sensors. The schematic of the test plate, sensor deployment and damage location are shown in Fig. 5(b). It should be noted that both damage types are shown in this schematic for demonstration purpose; in the actual experiments, two different plates, each with a single damage type, were used. To minimize the experimental noise and uncertainties, the final signal for each experiment was taken as the average value of 10 measurements.

4. Results and discussion

In order to obtain the optimal excitation configuration (i.e., the highest energy content), the highest amplitudes of signals in the excitation frequency range of 10 kHz to 110 kHz, extracted from the sensor with the shortest distance from the actuator, were compared. As shown in the Fig. 7, the signals with frequencies between 60 kHz and 80 kHz show relatively larger amplitudes compared with other regions, indicating higher energy content and more wave mode information. In this section, results of the healthy case under a 70 kHz excitation frequency, which is characterized by the developed algorithm, is shown in Section 4.1. The multi-dimensional signal processing and mode tracking approach are also demonstrated in this section, which includes signal de-noising, construction of TSR from original signals, and mode tracking approach for identifying the trajectory of each wave mode. The mode tracking approach associated with localization results with facesheet delamination under a 70 kHz excitation frequency are presented in Section 4.2. In addition, the results of foam core separation under a 70 kHz excitation frequency are presented in Section 4.3. Finally, taking advantage of the current framework's ability to track all wave modes present in the sensing signal, a mode conversion mechanism comparing facesheet delamination and foam core separation is also discussed in Section 4.3.

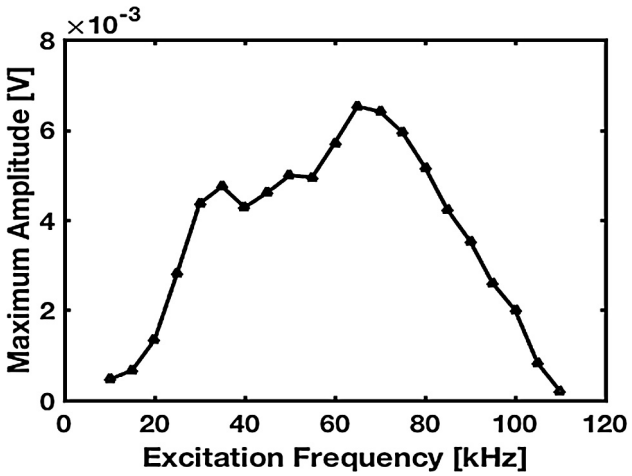

Fig. 7. Comparison of maximum signal amplitudes under varying excitation frequencies.

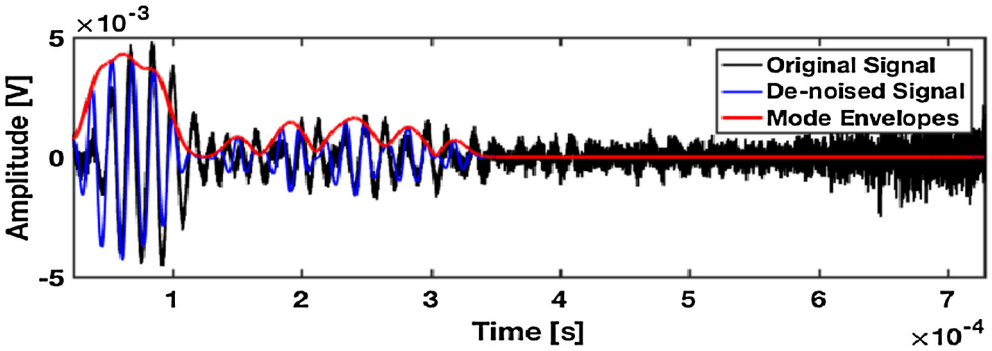

Fig. 8. Demonstration of MPD de-noising and Hilbert transform based envelope detection.

4.1. Healthy path

The reference-free perspective of developed algorithm, which is capable of identifying and localizing damage without baseline information, was experimentally validated. Each experimental scenario (healthy and damaged sensing paths) has been automatically classified; comparing with known damage locations, each damaged path could be successfully identified, and no healthy path could be identified as a damaged path. These results represent a successful demonstration of the multi-dimensional signal processing methodology and mode tracking approach proposed in this research. The results from the healthy path under a 70 kHz excitation frequency and associated processes for mode trajectory tracking are discussed in this section.

Fig. 8 is an illustration of the original signal from the sensor that is at the shortest distance from the actuator, i.e., sensor 5, along with its associated de-noised signal, based on the MPD methodology with 15 iterations and mode envelopes of the Hilbert transform based envelope detection equation, i.e., Eq. (8). It can be observed that each mode here is successfully extracted, while the noise is filtered, and wave modes isolated. The mode locations (i.e., peaks) of these signals in time domain are also identified, as shown in Fig. 9, and used to constructed TSR using Eqs. (10)–(13). As seen in Fig. 9, the sensors are marked from 1 to 5; sensor 5 is defined as the sensor that is at the shortest distance from the actuator and sensor 1 is the one that is at the longest distance. It should be noticed that waveforms from 0 s to 0.3×10^{-4} s in the signals presented in Fig. 9 are truncated, because the waveforms contained in this region are the echo of excitation signals, not the signals received by sensors, due to the synchronization method implemented in data acquisition system. The presence of the first peak in sensor 2 is also due to this issue, but it can be automatically eliminated by the developed algorithm.

The mode tracking approach described in Section 2.3 was then applied, and the group velocity and source location vector were identified. The reflected waves from the boundary were deliberately not taken into consideration in the current study; however, no wave source could be found except those in the actuating region in this healthy case. In order to find how many

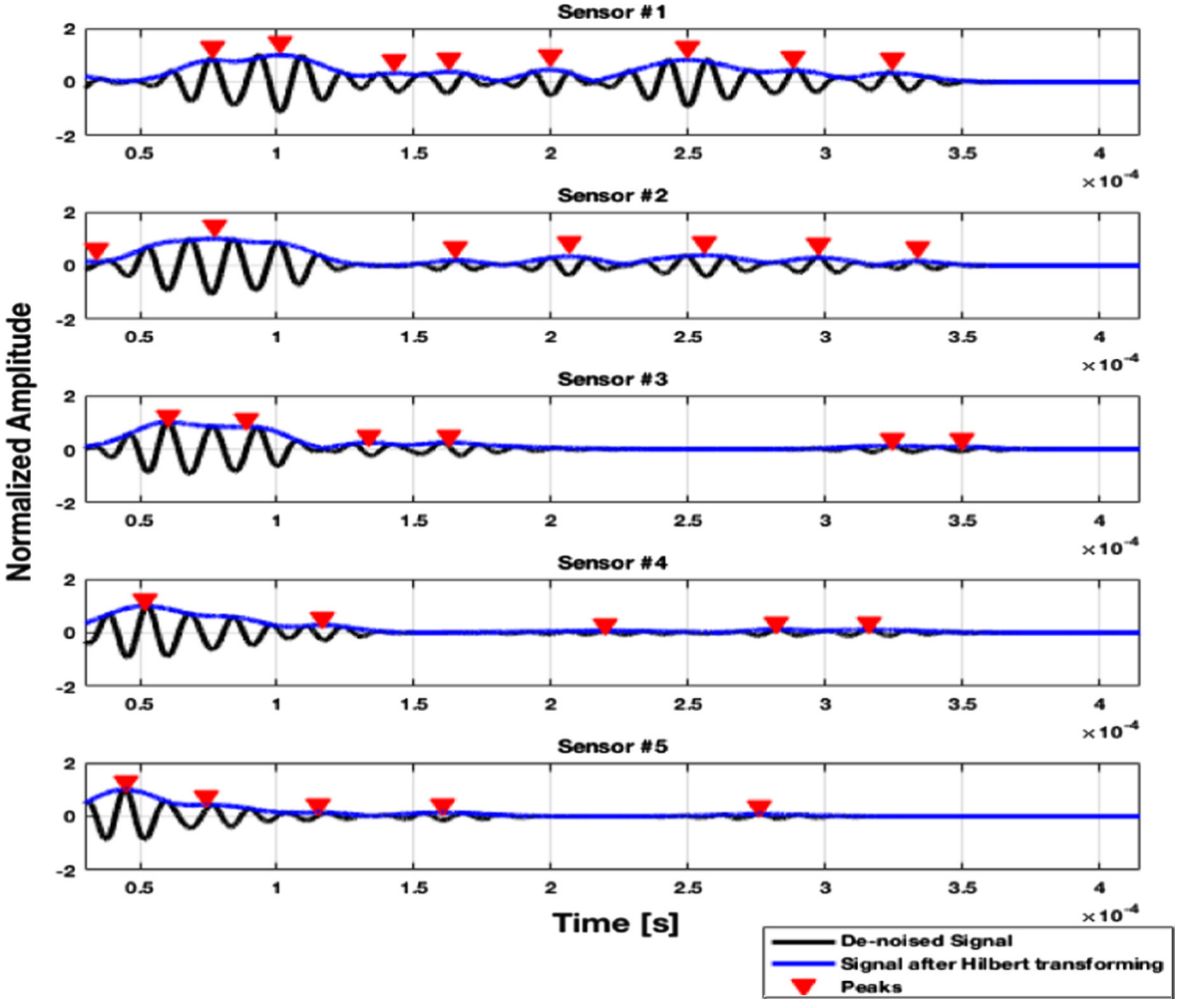

Fig. 9. Signals from sensors in healthy path with locations of wave mode peaks.

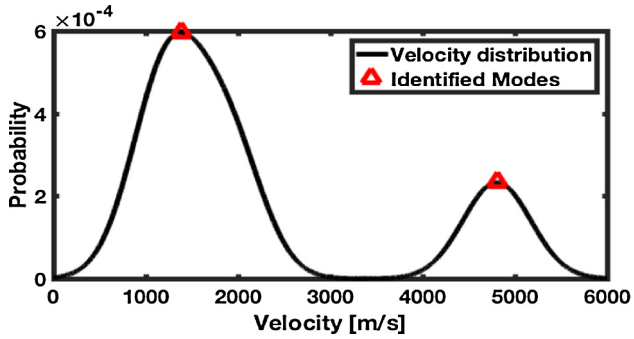

Fig. 10. Velocity distribution for identifying the number of UGW modes.

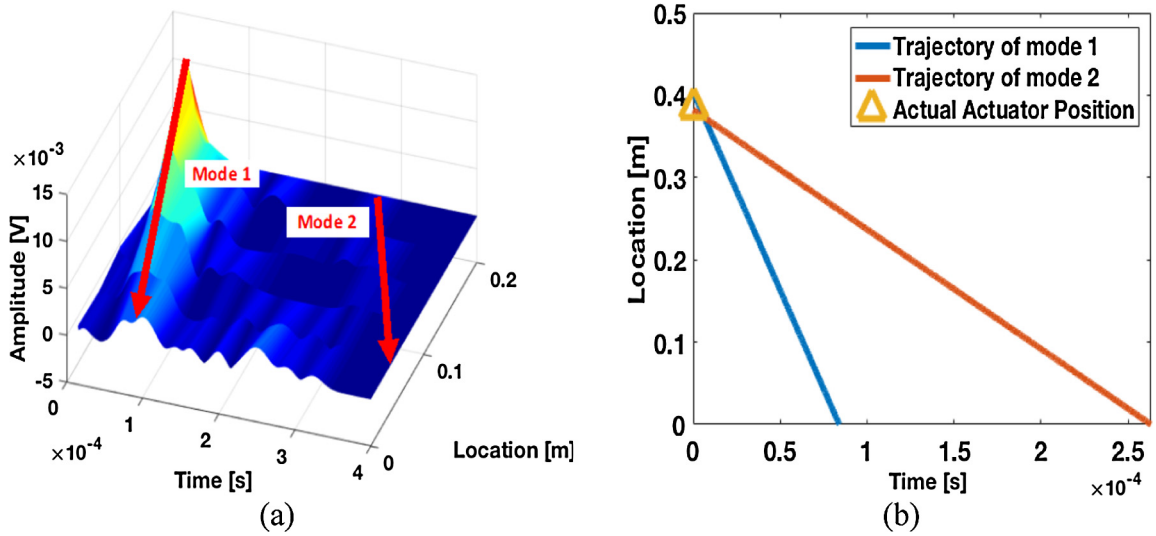

Fig. 11. (a) Three-dimensional TSR and the trajectories of two actuated wave modes; (b) top-view of the TSR with the predicted and actual locations of actuator.

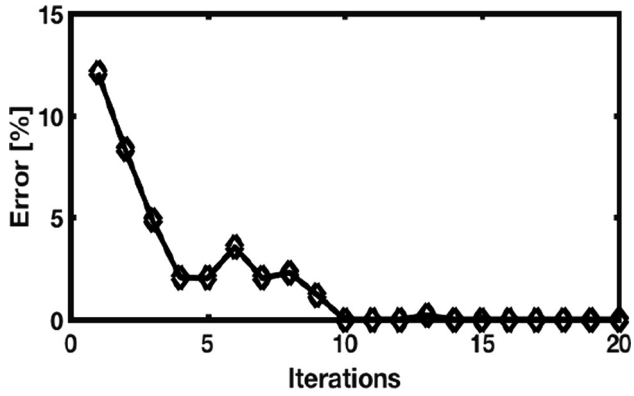

Fig. 12. Error of wave source location predicting for the actuator with respect to numerical iterations.

wave modes were present, the KDE was implemented, as introduced in Eq. (25). The results from 20 numerical iterations are shown in Fig. 10. It can be observed that there are two modes within the group velocity distribution. Using Eqs. (28)–(31), the group velocity and trajectories of these two wave modes can be found, and the locations of wave source were accurately predicted, when compared with the known location of actuators. The spatial origin of three-dimensional TSR, defined here

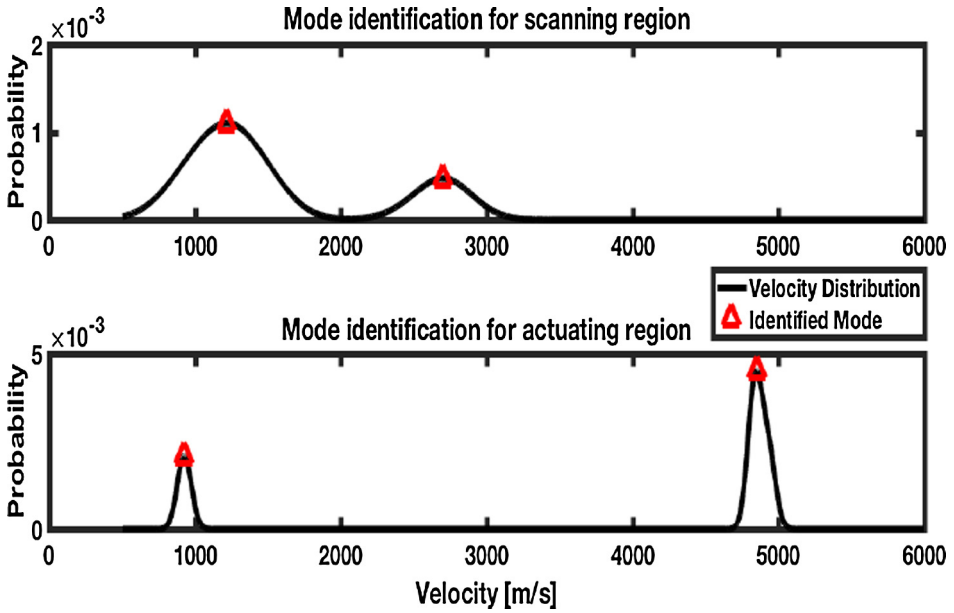

Fig. 13. Group velocity distributions for identifying the number of UGW modes in scanning region and actuating region with the presence of facesheet delamination.

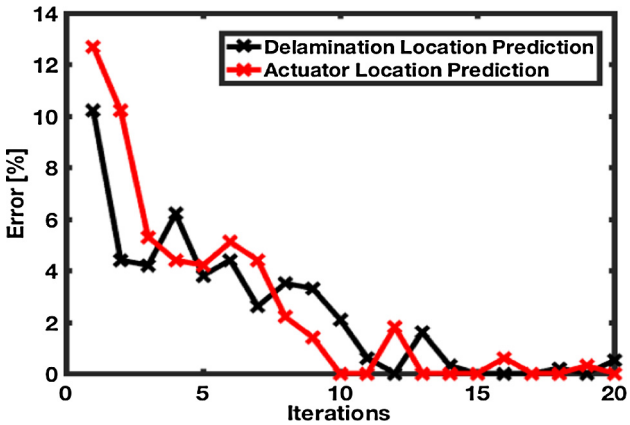

Fig. 14. Errors of wave source location predicting for the actuator and facesheet delamination with respect to numerical iterations.

as the location of sensor 1, which is the farthest sensor from the actuator but the closest to the boundary, is shown in Fig. 11 (a). The trajectories in time-space domain are presented in Fig. 11(b) with the actual location of the actuator. The group velocities of wave modes 1 and 2 are found to be 4805 m/s and 1381 m/s, respectively. Additional modes can also be found in the three-dimensional TSR, especially when the sensor is close to the boundary. These wave modes are regarded as the reflected waves from the boundary.

The error in predicting the actuator location with respect to the numerical iteration is shown in Fig. 12. Based on the sizes of MFC actuators, which is 28 mm in the direction of sensing path, the error is seen to be zero if the predicted location is in the actuating region; otherwise the errors were calculated based on Eq. (32), and the final error values represented the mean values of all the modes. Based on the above experimental set up, the results show that the developed algorithm can converge rapidly (within 10 numerical iterations) and predicts the wave source location very accurately.

4.2. Facesheet delamination

The developed algorithm was also able to successfully identify the sensing path with a facesheet delamination under a 70 kHz excitation frequency, and the results from 20 numerical iterations are presented in this section. In addition to the two wave modes from the actuator in the healthy case, two additional wave modes were detected in the scanning region (i.e.,

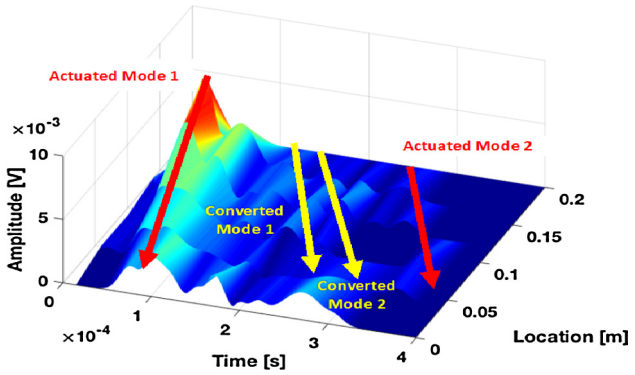

Fig. 15. Three-dimensional TSR and the trajectories of two actuated wave modes and two delamination induced converted wave modes.

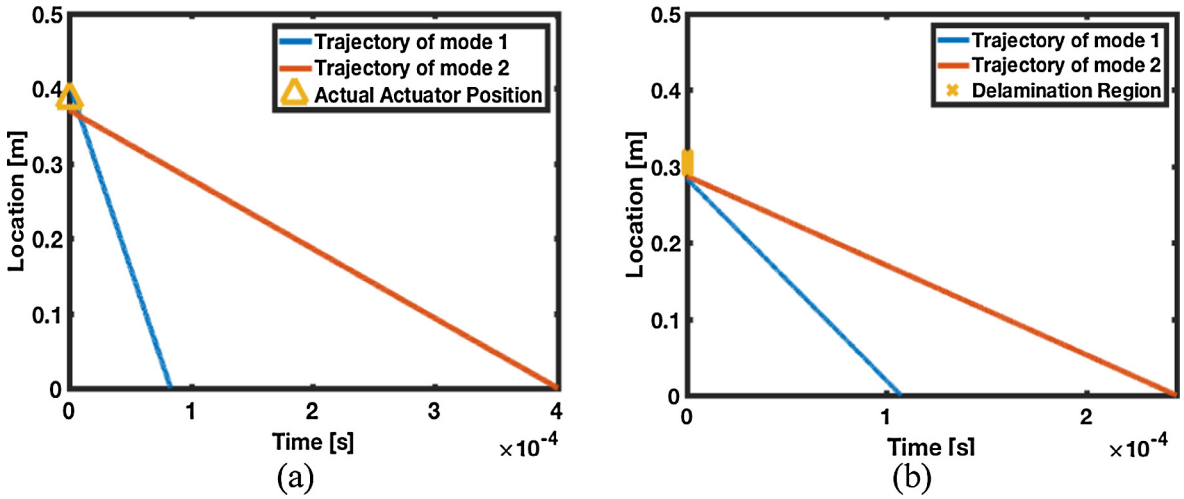

Fig. 16. Top-view of the TSR with the (a) predicted and actual locations of actuator, and (b) predicted and actual locations of facesheet delamination.

$\boldsymbol{K}_{Dam}$), as shown in the Fig. 13. The scanning region in this figure is defined as the region outside of the actuating region, but within the boundary known as $\boldsymbol{D}_{Dam}$. According to the sizes of facesheet delamination and the actuator, using the same approach as described in Section 4.1, error is plotted as the function of the number of numerical iterations is shown in Fig. 14, which indicates that the developed algorithm is robust in predicting the locations of actuators and delaminations in the current experimental setup.

The trajectories of all the wave modes, actuated and converted, in the time-space domain are shown in Fig. 15. The two-dimensional top-view of the wave mode trajectories are presented in Fig. 16. The velocities of the two modes from the actuating region were 926 m/s and 4849 m/s, indicating that the presence of the facesheet delamination had a minor impact on the velocities of the two modes transmitted from the actuator. The small discrepancies in the group velocities between the healthy path and the path with facesheet delamination were due to the quasi-isotropic nature of X-COR panel; the group velocities of wave modes containing the signals were dependent on the UGW propagating directions [4]. The velocities of the two converted waves induced by the facesheet delamination are 1218 m/s and 2699 m/s; both modes can be indicators of the delamination location.

4.3. Foam core delamination

The developed algorithm was able to identify the sensing path with a foam core separation under a 70 kHz excitation frequency. Fig. 17 shows that there were two actuated wave modes and two foam core separation induced converted wave modes presenting in the scanning region and actuating region respectively with 20 numerical iterations. According to the size of the actuator and the size of the foam core separation, as mentioned in Section 3, the errors shown in Fig. 18 indicate that the developed method converges rapidly with high accuracy. Similar to the facesheet delamination case, the prediction errors for both actuator and damage are seen to be very close to zero, within 10 numerical iterations. The full time-space domain is shown in Fig. 19 along with the trajectories of actuated and converted wave modes, while the two-dimensional top-view

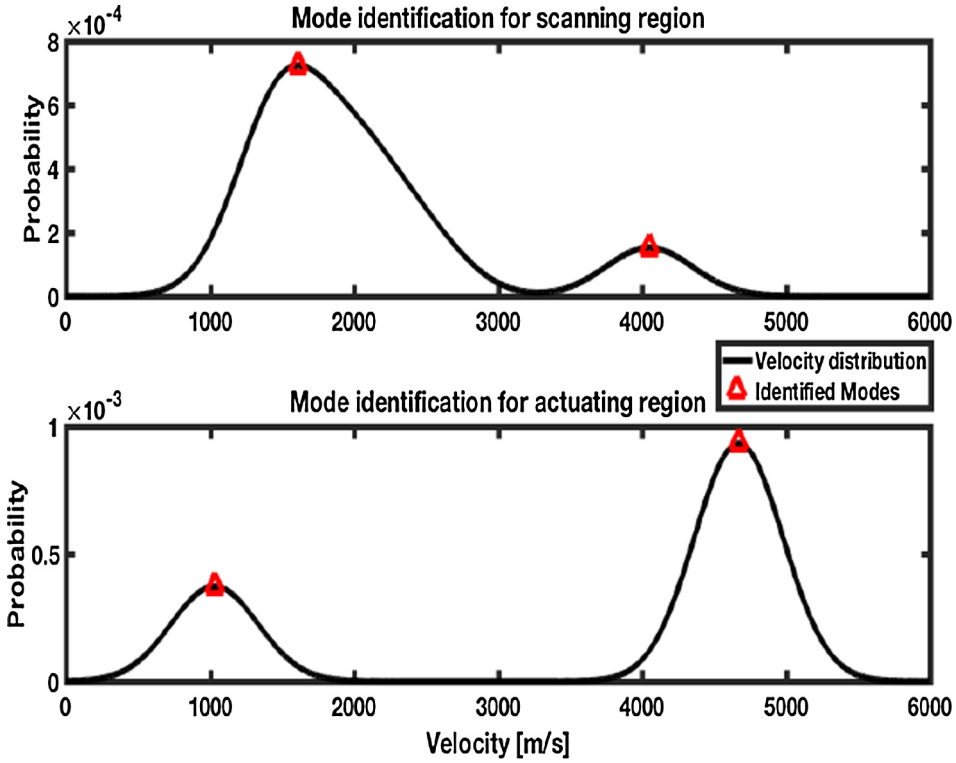

Fig. 17. Group velocity distributions for identifying the number of UGW modes in scanning region and actuating region with the presence of foam core separation.

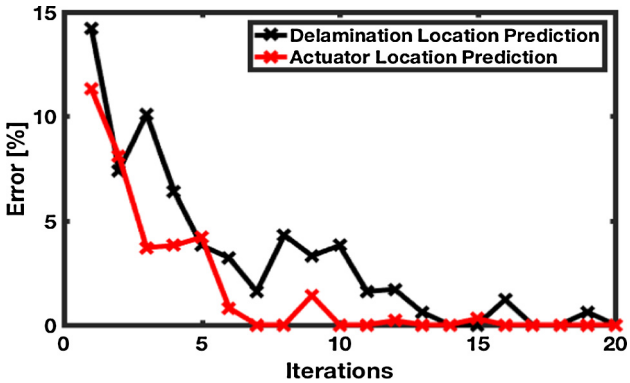

Fig. 18. Errors of wave source location predicting for the actuator and foam core separation with respect to numerical iterations.

of the wave mode trajectories are presented in Fig. 20. The velocities of the actuated modes were 1033 m/s and 4672 m/s, similar to the velocities of the actuated modes in both the healthy and facesheet delamination cases. This indicates that, as in the case of the facesheet delamination, the actuated wave velocities were not significantly impacted by the presence of foam core separation. Again, the small discrepancies were due to the quasi-isotropy of the X-COR panel. However, the velocities of two converted wave induced by the foam core separation were 1014 m/s and 4050 m/s, and the velocity of the relatively faster wave mode showed a significant difference compared to the facesheet delamination case (2699 m/s). It is important to note that: (1) The facesheet delamination is located at the mid-layer of the top facesheet and the foam core separation, which is located between facesheet and foam core; (2) The delaminated/separated interfaces of the two damage cases are between two composite layers and between a composite layer and a foam core layer, respectively. This indicates that the velocities of converted waves are strongly dependent on the location of damage in the through-thickness direction and the damage features (facesheet delamination and foam core separation).

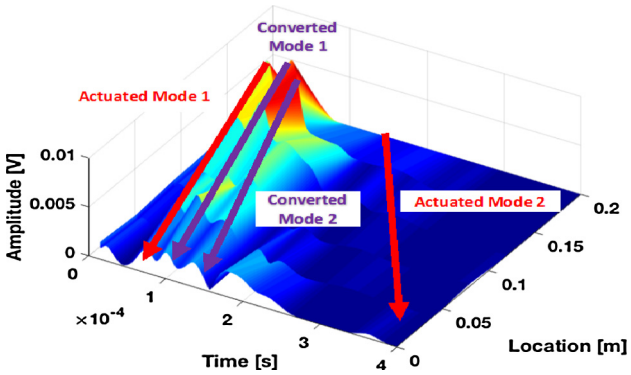

Fig. 19. Three-dimensional TSR and the trajectories of two actuated wave modes and two foam core separation induced converted wave modes.

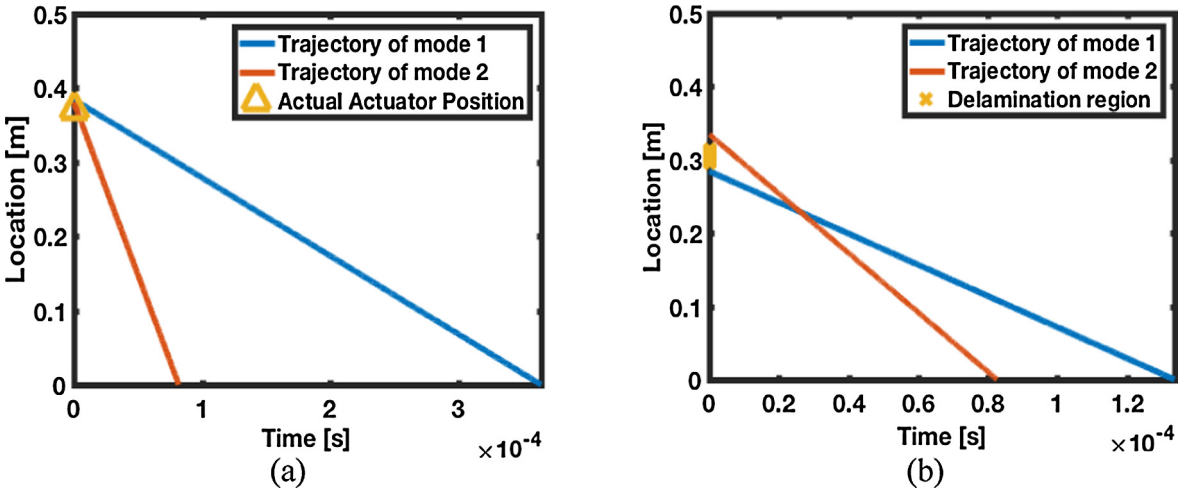

Fig. 20. Top-view of the TSR with the (a) predicted and actual locations of actuator, and (b) predicted and actual locations of foam core separation.

5. Concluding remarks

A robust multi-dimensional signal processing methodology and mode tracking approach were developed for UGW based structural health monitoring aiming at accurately localizing *in situ* damage in highly complex media that has an issue of large attenuation such as X-COR sandwich structures. This methodology is especially applicable in the context of the challenges involved in detecting damage-induced reflected waves. Instead of investigating a portion of waveforms in the time domain, the developed computation framework utilizes the full wave field in the time-frequency-space domain to locate wave sources with a reference-free perspective. The sensing signals were de-noised in the time-frequency domain associated with a Hilbert envelope detection technique and used to construct time-space domain by importing the spatial information of transducers. All possible wave mode trajectories were identified in the time-space domain and clustered using a KDE and K-means clustering methodology so that the source locations of all wave modes could be successfully located. The developed framework was then experimentally validated through X-COR panels with two damage scenarios (i.e., facesheet delamination and foam core separation). The results showed that both damage scenarios can be accurately identified. In addition, the mode tracking approach indicated that the presence of facesheet delamination and foam core separation did not significantly influence the velocities of actuated wave modes. Instead, the presence of damage resulted in the converted waves having completely different velocities under varying damage scenarios, while all the converted wave modes are proven to be effective damage location indicators. Therefore, the developed method is not only an effective damage localization methodology but is also capable of providing important insights into the complex behaviors of UGW in complex and heterogeneous structures. Future work will involve developing a sensor optimization method that can reduce the number of sensors while maintaining high localization accuracy.

Acknowledgement

The authors would like to gratefully acknowledge the Adaptive Intelligent Materials and Systems (AIMS) center with the co-sponsor, The Boeing Company, for funding this work through the Industry Consortium Core Project. The authors appreciate the continuous guidance and help, including access to the facility for fabrication of the X-COR panels, from technical monitor, Dr. Daniel W Huff.

References

[1] L. Du, G. Jiao, Indentation study of Z-pin reinforced polymer foam core sandwich structures, Compos. Part Appl. Sci. Manuf. 40 (2009) 822–829.
[2] T.K. O'Brien, I.L. Paris, Exploratory investigation of failure mechanisms in transition regions between solid laminates and X-cor® truss sandwich, Compos. Struct. 57 (2002) 189–204.
[3] Y. Li, X. Jun, Y. Tan, Y. Yuan, X. Dang, Study on compressive properties of X-COR sandwich structures, Acta Aeronautica Et Astronautica Sinica 3 (2009) 025.
[4] V. Giurgiutiu, Structural Health Monitoring: with Piezoelectric Wafer Active Sensors, Academic Press, 2007.
[5] A. Raghavan, C.E.S. Cesnik, Finite-dimensional piezoelectric transducer modeling for guided wave based structural health monitoring, Smart Mater. Struct. 14 (2005) 1448.
[6] Z. Su, L. Ye, Y. Lu, Guided Lamb waves for identification of damage in composite structures: a review, J. Sound Vib. 295 (2006) 753–780.
[7] P.S. Tua, S.T. Quek, Q. Wang, Detection of cracks in plates using piezo-actuated Lamb waves, Smart Mater. Struct. 13 (2004) 643.
[8] S.S. Kessler, S.M. Spearing, C. Soutis, Damage detection in composite materials using Lamb wave methods, Smart Mater. Struct. 11 (2002) 269.
[9] M. Kehlenbach, S. Das, Identifying damage in plates by analyzing Lamb wave propagation characteristics, in: Smart Nondest. Eval. for Health Monit. of Struct. and Bio. Syst., 2002, pp. 364–375
[10] J. Moll, R.T. Schulte, B. Hartmann, C.-P. Fritzen, O. Nelles, Multi-site damage localization in anisotropic plate-like structures using an active guided wave structural health monitoring system, Smart Mater. Struct. 19 (2010) 45022.
[11] S.H. Díaz Valdés, C. Soutis, Real-time nondestructive evaluation of fiber composite laminates using low-frequency Lamb waves, J. Acoust. Soc. Am. 111 (2002) 2026–2033.
[12] R.K. Neerukatti, K. Hensberry, N. Kovvali, A. Chattopadhyay, A novel probabilistic approach for damage localization and prognosis including temperature compensation, J. Intell. Mater. Syst. Struct. 27 (2016) 592–607.
[13] V. Giurgiutiu, J. Bao, A.N. Zagrai, Structural health monitoring system utilizing guided lamb waves embedded ultrasonic structural radar, US6996480 B2, 2006.
[14] S.S. Kessler, S.M. Spearing, M.J. Atalla, C.E.S. Cesnik, C. Soutis, Damage detection in composite materials using frequency response methods, Compos. Part B Eng. 33 (2002) 87–95.
[15] A. Żak, M. Krawczuk, W. Ostachowicz, Vibration of a laminated composite plate with closing delamination, J. Intell. Mater. Syst. Struct. 12 (2001) 545–551.
[16] H.S. Kim, J. Kim, S.B. Choi, A. Ghoshal, A. Chattopadhyay, Modal-strain-based damage index of laminated composite structures using smooth transition of displacements, AIAA J. 45 (12) (2007) 2972.
[17] Y. Liu, M.Y. Fard, A. Chattopadhyay, D. Doyle, Damage assessment of CFRP composites using a time–frequency approach, J. Intell. Mater. Syst. Struct. 23 (2012) 397–413.
[18] I. Kim, A. Chattopadhyay, Guided Lamb wave–based structural health monitoring using a novel wave packet tracing method for damage localization and size quantification, J. Intell. Mater. Syst. Struct. 26 (2015) 2515–2530.
[19] T.E. Michaels, J.E. Michaels, M. Ruzzene, Frequency–wavenumber domain analysis of guided wavefields, Ultrasonics 51 (2011) 452–466.
[20] L. Yu, Z. Tian, Lamb wave structural health monitoring using a hybrid PZT-laser vibrometer approach, Struct. Health Monit. 12 (2013) 469–483.
[21] L.H. Yam, Y.J. Yan, J.S. Jiang, Vibration-based damage detection for composite structures using wavelet transform and neural network identification, Compos. Struct. 60 (2003) 403–412.
[22] H. Sohn, D. Dutta, J.Y. Yang, H.J. Park, M. DeSimio, S. Olson, E. Swenson, Delamination detection in composites through guided wave field image processing, Compos. Sci. Technol. 71 (2011) 1250–1256.
[23] R.K. Neerukatti, A. Rajadas, L. Borkowski, A. Chattopadhyay, D.W. Huff, A hybrid method for damage detection and quantification in advanced X-COR composite structures, in: >Sensor and Smart Struct. Tech. for Civil, Mech., and Aero. Syst., 2016, pp. 980326-980326-16.
[24] K. Diamanti, C. Soutis, J.M. Hodgkinson, Lamb waves for the non-destructive inspection of monolithic and sandwich composite beams, Compos. Part Appl. Sci. Manuf. 36 (2005) 189–195.
[25] G. Li, R.K. Neerukatti, A. Rajadas, A. Chattopadhyay, D. Huff, Guided wave based damage assessment in X-COR composite sandwich structures, in: 25th AIAAAHS Adapt. Struct. Conf., American Institute of Aeronautics and Astronautics, 2017, p. 1679.
[26] S.G. Mallat, Z. Zhang, Matching pursuits with time-frequency dictionaries, IEEE Trans. Signal Process. 41 (1993) 3397–3415.
[27] T.J. Ulrich, Envelope calculation from the Hilbert transform, 2006.
[28] D. Chakraborty, Time-frequency based adaptive learning for structural health management, Arizona State University, (Ph.D)., 2010.
[29] L. Yu, V. Giurgiutiu, Advanced signal processing for enhanced damage detection with piezoelectric wafer active sensors, Smart Struct. Syst. 1 (2) (2005) 185–215.
[30] K. Worden, G. Manson, D. Allman, Experimental validation of a structural health monitoring methodology: Part I. Novelty detection on a laboratory structure, J. Sound Vib. 259 (2) (2003) 323–343.
[31] J.A. Hartigan, M.A. Wong, Algorithm AS 136: A K-means clustering algorithm, J. R. Stat. Soc. Ser. C Appl. Stat. 28 (1979) 100–108.
[32] G. Li, A. Rajadas, A. Chattopadhyay, D.W. Huff, A reference-free guided wave based damage localization approach for highly dispersive structures, Struct. Health Monit. 2017 (2017) 1607–1614.